Theoretical and experimental study of uv lasers in Be-like ions pumped by resonant photoexcitation

Niansheng Qi* and Mahadevan Krishnan†
Section of Applied Physics, Yale University, New Haven, Connecticut 06520
(Received 6 July 1988)

A uv laser based on resonant photoexcitation is described. This type of laser is a prototype for soft-x-ray lasers in isoelectronic analogs. Intense, Mn VI–line radiation at 310 Å from a CO_2-laser-produced plasma was used to resonantly pump C III ions, in an adjacent vacuum-arc discharge, from the $2s^2$ ground state to the $2s4p$ upper level. Electron collisions rapidly redistribute the population of the pumped $4p$ level among other $n=4$ levels. Enhanced fluorescence coincident with the Mn VI–line radiation was observed on many 4-3 transitions in C III. To describe the kinetics in C III ions, a 72-level collisional radiative model was constructed with up-to-date atomic data. Measured values of electron density and temperature in the C and Mn plasmas were used as inputs to the model. To verify this model, the populations of excited states in C III ions were measured spectroscopically and compared with predictions. Gain coefficients of about 0.1 cm^{-1} were predicted by the model. These gains were found to be consistent with the experiments. Single-pass gain measurements showed that the total gain-length product was 0.5 in two C III lines at 2177 and 2163 Å. Laser action at these wavelengths was demonstrated in a resonant Fabry-Perot cavity. This C III–Mn VI photoexcitation scheme is a prototype for soft-x-ray lasers in higher Z, isoelectronic analogs, such as Mg IX–Al XI and others.

I. INTRODUCTION

Much effort has recently been concentrated on finding suitable processes for producing a laser radiating at wavelengths in the vacuum ultraviolet region and below.[1–4] Short-wavelength lasers might find applications in plasma diagnostics, fusion research, contact microradiography, and in spectrochemical analysis.[5–7] There are many approaches to soft-x-ray lasers. Population-inversion mechanisms include direct collisional excitation,[8–11] three-body or dielectronic recombination,[12–16] broadband inner-shell photoexcitation,[17–19] and resonant photoexcitation.[20–22] Recently, high gain at soft-x-ray wavelengths has been demonstrated in Ne-like[23,24] and Ni-like,[25] laser-produced plasmas. Inversions between the $2p^53p$ and $2P^53s$ levels in Ne-like ions appear to be driven by a combination of direct collisional excitation from the $2p^6$ ground state as well as dielectronic recombination from the F-like $2p^5$ ground state. The search for a three-body recombination-pumped laser has produced noteworthy results[26–29] in C VI at 182 Å, in a laser-produced plasma, with or without magnetical confinement. A third approach to soft-x-ray lasers is by resonant photoexcitation of ions in one plasma by intense, line radiation from ions in an adjacent plasma. In this scheme, electrons are pumped from the ground state of the pumped species to an excited state by resonant photoexcitation. Population inversions can be produced between this excited level and lower-lying intermediate levels.

Selective photoexcitation offers several advantages. Population inversion can be effectively enhanced using selective photoexcitation of the upper level of the lasing ion with charge state Z_l by a broadened resonance line from ions with charge state Z_p ($Z_p > Z_l$) in a two-component plasma. For a sufficiently intense pump line, the pumped level can be driven into equilibrium with the pump radiation field, and the population of the pumped level is characterized by the temperature of the pump plasma, while the other levels of the pumped ion are characterized by the temperature of the pumped medium. Because $Z_p > Z_l$, it is possible to have the temperature $T_p > T_l$ and to provide significantly higher effective temperature of excitation in the pumped (lasing) plasma.

Optical pumping using intense line radiation from one ion species to pump a different ion species was first achieved[30] in 1930. Enhanced fluorescence at 3.2 μm in Cs I was observed, using 3880 Å pump-line radiation from He I. In 1961, such resonant photoexcitation led to laser oscillation[31] at 3.2 μm. Using photoexcitation of He atoms and then collisional transfer to the high-lying levels of neon, Lisitsyn, Fedchenko, and Chebotayev[32] reported laser oscillation at 1.8, 1.6, and 1.3 μm in Ne I. The concept was extended[33] to 5461 Å in Hg I, using two-step photoexcitation. The principal difficulty arising in resonant photoexcitation lasers is to find resonances between the pump and pumped transitions. These resonances must be within the width of the corresponding transitions. Poor coupling due to the wavelength mismatch between the pump and the pumped lines can be reduced by using an opacity broadened pump line. But then the efficiency is low because only a small fraction of the pump line is effective. The first published proposal concerning the extension of this approach into the xuv and soft-x-ray regimes is that of Vinogradov, Sobelman, and Yukov,[20] who in 1975 proposed a number of candidate resonance matches between one- and two-electron

ions of moderately low Z. One of these proposed schemes uses the Si XIII 6.65-Å line to pump Al XII at 6.635 Å. Lasing is predicted at 44 Å. Norton and Peacock[21] proposed to use the C VI $2p$-$1s$ resonance line at 33.74 Å to pump the 1-4 singlet line at 33.43 Å in C V yielding an inversion at 186.7 Å in C V. Due to the magnitude of the wavelength mismatch, additional broadening of the pump line was required. It was suggested that opacity would lead to linewidths great enough to overcome the mismatch. Bhagavatula suggested using C VI to pump Mg XII with lasing at 130 Å.[34] Several other resonant photoexcitation schemes in H-like and He-like ions have been proposed[10] and analyzed,[22] and some experiments[35,36] have been reported. Recently, Krishnan and Trebes[37] proposed a class of photoexcitation lasers in Be-like ions. Quasi-cw lasers with wavelengths from 2177 Å in C III pumped by Mn VI–line radiation to 230 Å in Mg IX pumped by Al XI were identified, in an isoelectronic sequence. Since C III is isoelectronic with Mg IX, the collisional radiative kinetics elucidated by this research shed light on possible soft-x-ray lasers in Mg IX.

Figure 1 illustrates the principle of resonant photoexcitation. Intense Mn VI–line radiation at 310.182 Å pumps the C III ions from the $2s^2$ ground state to the $2s4p$ upper level. The 0.012-Å wavelength mismatch is small enough to be overcome by Doppler broadening of the Mn VI pump line. For intense Mn VI–line radiation, inversion occurs in C III between $4p$ and $3d$, and a laser is possible at 2177 Å. Collisions in the C III plasma may rapidly thermalize the $n=4$ level populations. In this case, gain is also possible on other $n=4$ to $n=3$ transitions as shown in the figure. In the experiments, the C III ions were produced in a vacuum-arc discharge with electron temperature of 4 eV and electron density of $\sim 5\times 10^{15}$ cm^{-3}. The pump Mn VI–line radiation was produced in a dense and hot laser-produced Mn plasma adjacent to the C plasma. Photoexcitation was inferred by monitoring enhanced fluorescence on the $n=4$ to $n=3$ transitions. The lifetime of the upper $n=4$ levels is longer than the lower $n=3$ levels so that quasi-cw population inversion can be expected on $n=4$ to $n=3$ transitions. With this as an introduction, let us turn to the substance of this paper.

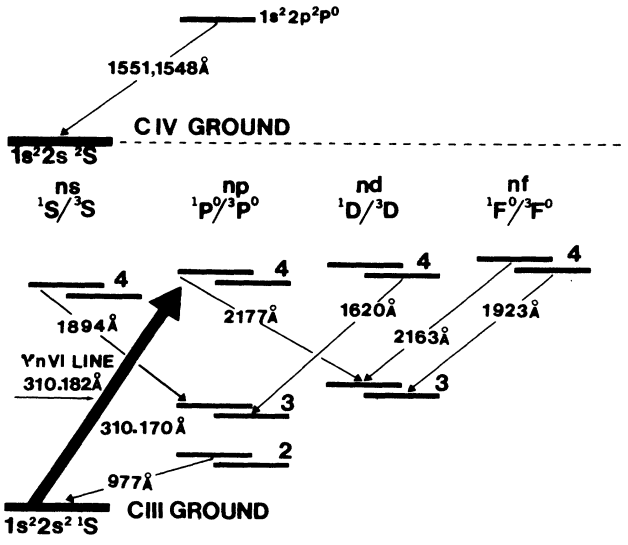

FIG. 1. Schematic Grotrian diagram illustrating selective photoexcitation Mn VI–C III laser scheme.

The rest of the paper is organized as follows. In Sec. II a computer simulation of the Mn VI–C III scheme is presented. The object of this model is to provide design criteria for an experiment to demonstrate a photoexcited laser in C III. Ionization charge states of carbon ions are calculated by a modified coronal model. A 72-level collision radiative model is developed for C III ions in excited states. The model is extended to take account of the selective photopumping from a Mn pump plasma by including stimulated emission and reabsorption due to the Mn VI–pump-line radiation (with an estimated 20-eV brightness temperature). Using this model, the optimal conditions for population inversions in C III excited states are obtained. Section III presents a spectroscopic study of the carbon discharge. Measurements of electron density and temperature in the C plasma, using line profiles and absolute intensities of emitted C II and C III lines, are discussed. The collisional radiative model is compared with absolute-intensity measurements of some C III lines. Section IV describes the experiments conducted for measuring fluorescence and gain. Laser action at 2177 and 2163 Å in C III is described. In Sec. V the results obtained are summarized and their implications for future work are discussed.

II. MODEL OF THE Mn VI–C III PHOTOEXCITATION SCHEME

To achieve population inversions the plasma conditions required for the carbon and manganese plasmas are quite different. In the C plasma most ions should be in the C III ground state, while in the pump Mn plasma, most ions are desired in the Mn VI charge state. One must determine what densities and temperatures in the two separate plasmas would provide ideal lasing conditions. Determining the conditions for population inversion requires the investigation of the C III level populations prior to and during photoexcitation. To provide this information, the kinetics of the pumped carbon plasma are studied by a collisional radiative model, in which the plasmas is assumed to be a homogeneous, stationary, and charge neutral medium.

The calculation of the excited state populations in C III is carried out in two steps. First, a modified coronal ionization balance is used to calculate the total populations of the $C, C^+, \ldots, C^{6+}$ charge states, which include the total populations of the ground and/or metastable states. The populations are dependent on the electron density and the electron temperature. Then, a collisional-radiative model for C III ions in excited states is constructed, in which populations of C III and C IV ground states are supplied as inputs from the ionization balance. The approximation of calculating the ground states of carbon ions first and the excited states of C III separately

is valid, when most ions are in the ground and metastable states. This reduces the number of the rate equations dramatically so that it allows the treatment of each ion charge state without recourse to lengthy computation.

The ionization balance model describes the net effect of the ionization and recombination processes in the carbon ions. In the steady-state case, the ionization balance is given by

$$\frac{N_z}{N_{z+1}} = \frac{\alpha_{z+1} N_e + \beta_{z+1} + D_{z+1}}{S_z} , \tag{1}$$

where N_e is the electron density, N_z is the population of the ion of charge z, S_z are the collisional ionization coefficients[38] from charge state z to $z+1$, and α_{z+1}, β_{z+1}, and D_{z+1} are the collisional,[39] radiative,[40] and dielectronic[41] recombination coefficients from the charge state $z+1$ to z, respectively. Notice that all the rate coefficients are independent of N_e except the three-body recombination rate coefficients, which are proportional to N_e. In the intermediate density range, collisional recombination is negligible. The normalized densities N_z/N_e are predominantly dependent on the electron temperature and slightly dependent on the electron density due to the weak density dependence of dielectronic recombination. The calculated relative abundance of carbon-ion charge states as a function of electron temperature is shown in Fig. 2. In the region of electron temperature from 3.5 to 8 eV, ions are highly populated in the C III charge state as shown in Fig. 2. The maximum C III ion abundance of 80% occurs at $T_e = 5$ eV.

The populations of the excited states in C III are calculated by a 72-level, collision-radiative (CR) model, which can be written as

$$\begin{aligned}\frac{dn_j}{dt} = &- \left[S_j N_e + \sum_{\substack{i,j \\ i<j}} (C_{ji}^d N_e + \Lambda_{ji} A_{ji}) + \sum_{\substack{i,j \\ i>j}} C_{ji}^e N_e \right] n_j \\ &+ \left[\sum_{\substack{i,j \\ i>j}} (C_{ij}^d N_e + \Lambda_{ij} A_{ij}) + \sum_{\substack{i,j \\ i<j}} C_{ij}^e N_e \right] n_i \\ &+ (\beta_j + \alpha_j N_e) N_e n_g^{3+} , \end{aligned} \tag{2}$$

where N_e is the electron density, n_g^{3+} is the ground-state population of C IV ions, and n_j is the population of the jth excited level. The C_{ji}^e and C_{ji}^d are the electron collisional excitation and deexcitation rate coefficients, respectively. The S_j, α_j, and β_j are the collisional ionization,[42–44] collisional recombination, and radative recombination[45] rate coefficients, respectively. A_{ji} is the spontaneous transition probability. Λ_{ji} is the Biberman-Holstein escape factor.[46,47] In the optically thin case, $\Lambda_{ji} = 0$. In the optically thick case, a 1-cm optical-path length is assumed. [Spatially resolved emission measurements, not described here, gave a full width at half maximum (FWHM) for the visible-uv emission of 1 cm.]

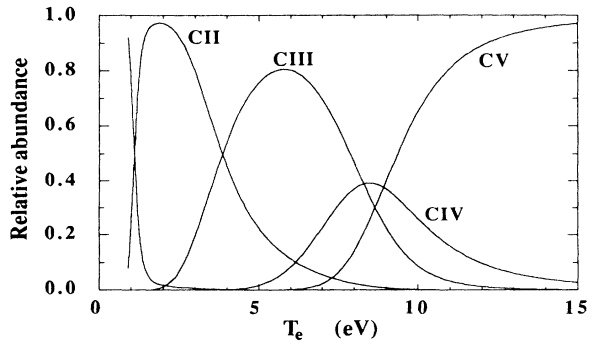

FIG. 2. Relative C ion charge state abundance as a function of electron temperature.

In the model, all singlet and triplet states of the outer electron configurations, with principal quantum numbers $n = 2-6$, are included. For $n = 7-9$, single lumped states distinguished only by principal quantum number n are treated. For sufficiently large principal quantum number, the levels are in local thermodynamic equilibrium (LTE) with each other. Griem[48] provides a formula for estimating the quantum number j of such levels, viz.,

$$N_e > 1.7 \times 10^{14} T_e^{1/2} \Delta E_j^3 , \tag{3}$$

where ΔE_j is the energy difference in eV between the C^{3+} ground state and the jth level. At $N_e = 5 \times 10^{15}$ cm^{-3} and $T_e = 4$ eV, j is approximately equal to eight. In the model, levels whose principal quantum numbers are greater than 9 are assumed in LTE with the C IV ground state under these conditions.

For levels from $n = 2$ to $n = 6$, the energy of each level, the radiative transition probability, and collisional excitation and deexcitation rates were provided by Morgan.[49] Hydrogenic rates[50,51] are used for the transitions involving $n \geq 7$ levels.

Using the rates discussed above, the rate equation (2) can be written in matrix notation as

$$\frac{dn}{dt} = An + n_g^{3+} R + n_g^{2+} E , \tag{4}$$

where A is the 71×71 matrix containing the rate coefficients linking the excited levels. n is the 71×1 column vector of level populations. The column vectors of R (71×1) and E (71×1) contain all recombination rates from the C IV ground state, and $n \geq 10$ levels and the excitation rates from the C III ground state, respectively. Since the relaxation times for the excited levels are much shorter than the time scales for evolution of the C III and C IV ground states, the excited-level populations maintain quasi-steady-state values.

To measure plasma conditions, i.e., N_e and T_e, it is desirable to find certain line ratios which are sensitive only to one of these parameters. Figure 3 shows the calculated line ratio of C III(4647 Å) to C III(3609 Å) as a function of T_e at several electron densities without optical trapping and Fig. 4 shows this ratio with the opacity included. At high electron temperatures this ratio is insensitive to T_e, while at low electron temperatures the ratio is weakly dependent on N_e. The advantage of using these lines is that no vacuum is needed for the spectrometer, whose absolute-intensity calibration in the visible region is straightforward and more accurate. Also, these

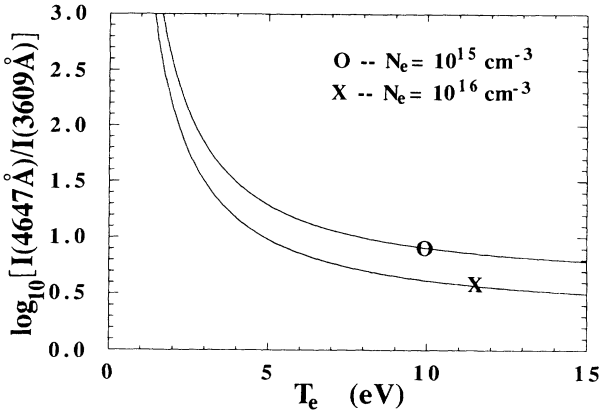

FIG. 3. Intensity ratio of C III lines at 4647 and 3609 Å as a function of electron temperature, at several electron densities.

lines are optically thin ($N_e < 5\times10^{16}$ cm^{-3}) such that it eliminates the uncertainty in measured line intensities due to opacity. The absolute intensity measurements of these two lines and their role in determining the plasma conditions are discussed in Sec. III.

So far the model has excluded selective photoexcitation in C III. When the C III ions are pumped by Mn VI–line radiation, the rate equations need to be modified. The photopumping adds two processes, stimulated emission and absorption for the transition $4p$-$2s$ in the CR model due to the presence of the selective photoexcitation, i.e., Eq. (2) is modified to read

$$\frac{dn_{4p}}{dt} = P(T_{\mathrm{Mn}})n_{2s} + \text{other terms}\ , \tag{5}$$

where $P(T_{\mathrm{Mn}})$ is the pumping rate due to the Mn VI–line radiation. The absorption fraction of the pumping radiation by the carbon plasma is estimated to be about 0.2 using a 1-cm optical-path length for the C III 310-Å line at an electron density of 10^{16} cm^{-3}. The pumped medium is, therefore, optically thin and the pump radiation penetrates the carbon plasma. An expression for the pumping rate is obtained by characterizing the optically thick Mn VI pump line with a brightness temperature T_{Mn}. The solid angle subtended by the observed volume to the Mn plasma is estimated to be π steradians and both the Mn VI pump line and the C III absorption line are assumed to be Doppler broadened. The desired expression is then

$$P(T_{\mathrm{Mn}}) = \tfrac{3}{4} A_{4p,2s} \frac{\Delta\lambda_p}{(\Delta\lambda_a^2+\Delta\lambda_p^2)^{1/2}} \times \frac{\exp\{-\ln(2)[\Delta\lambda^2/(\Delta\lambda_a^2+\Delta\lambda_p^2)]\}}{\exp(\Delta E/T_{\mathrm{Mn}})-1}\ , \tag{6}$$

where $\Delta\lambda$ is the wavelength mismatch between the pump and absorption lines, and $\Delta\lambda_a$ and $\Delta\lambda_p$ are the Doppler widths of the C III and Mn VI lines, respectively. Equation (6) assumes $n_{4p}/n_{2s} \ll 1$, which is true for all $T_{\mathrm{Mn}} \leq 20$ eV. In order to achieve a high population inversion, the brightness temperature T_{Mn} of the pump Mn VI line should be comparable to the energy ΔE ($\sim$39 eV) of the $4p$-$2s$ transition. For the typical laser-produced Mn plasma which was used in our experiments, a 20-eV brightness temperature for the Mn VI–pump-line radiation is a reasonable estimate.[52] At this brightness temperature $T_{\mathrm{Mn}}=20$ eV, the pumping rate $P(T_{\mathrm{Mn}})$ is 9.5×10^7/s. The enhancements of the excited-level populations as a result of optical pumping were calculated for various electron densities and temperatures of the C plasma with a fixed pumping rate, i.e., $T_{\mathrm{Mn}}=20$ eV. The maximum gain occurs at 4 eV. This temperature is lower than that of peak concentration of C III ions, but is a compromise between the conflicting need to maximize C III fraction while minimizing the deleterious excitation and ionization out of the $n=4$ levels. Figure 5 shows the populations of $4p\ ^1P^\circ$, $4s\ ^1S$, and $4f\ ^1F^\circ$ states versus N_e at an electron temperature of 4 eV. The dashed lines are the populations without photoexcitation and the solid lines with photoexcitation. The calculation indicates that the $4p$ population can increase by a factor of 160 due to optical pumping. At this density, the $4p$-$3d$ transition

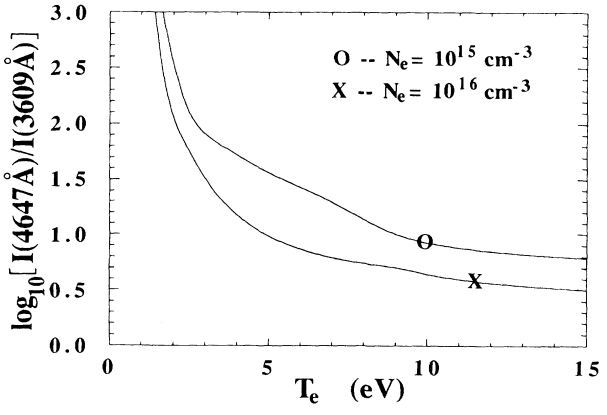

FIG. 4. Intensity ratio of C III lines at 4647 and 3609 Å as a function of electron temperature, assigning a 1.0-cm optical-path length.

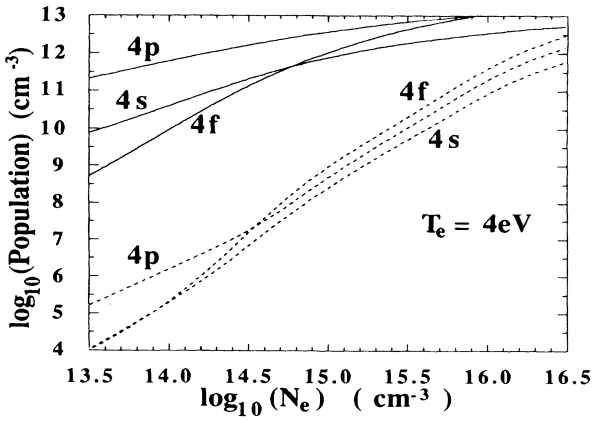

FIG. 5. Calculated populations of $n=4$ levels in C III. The solid lines are the enhanced populations due to resonant photoexcitation and the dashed lines are without photopumping.

line at 2177 Å is optically thin. The increase in density of the $4p$ level results in a similar increase in emission line intensity above the spontaneous emission level. Furthermore, rapid thermalization of the $n=4$ levels was predicted by the calculation. The population ratio n_{4p}/n_{4s} is weakly dependent on electron density. This reveals that the collisional coupling between the two levels is greater than radiative decay processes. Due to the strong radiative decay of the $4f$-$3d$ transition, the ratio of populations n_{4p}/n_{4f} is dependent on N_e. Thermal equilibrium occurs between $4p$ and $4f$ levels only when $N_e > 10^{16}$ cm^{-3}, as shown in Fig. 5.

The gain of a transition from upper level i to lower level j is defined, for a Doppler-broadened C line, as

$$G = 5.54\times10^{-32}\lambda^3 A_{ij}(n_i - n_j g_i/g_j)T_e^{-1/2} \text{ cm}^{-1} , \quad (7)$$

where λ is the transition wavelength in Å, A_{ij} is the transition probability, n_i and n_j are the populations of levels i and j, respectively, and g_i and g_j are the statistical weights of the levels. Figure 6 shows gain versus N_e at 2177, 2163, and 1894 Å, calculated at $T_e=4$ eV, without optical trapping. At low electron density, the ground-state density is much lower. Fewer electrons can be pumped from the ground state to the upper $4p$ level and then collisionally transferred to other $n=4$ levels. As a result, the gain is small. As the electron density increases, the ground-state population of C III is increased. The gain increases towards a peak value. At still higher electron densities $\sim 10^{16}$ cm^{-3}, electron collisions spoil the population inversion, as shown in Fig. 6. Due to the rapid collisional thermalization between the lower transition levels ($3p$ and $3d$) and between the upper transition levels ($4s$ and $4p$), the gain profile of the $4s$-$3p$ transition is similar to that of the $4p$-$3d$ transition. The gain reaches peak values of 0.13 and 0.10 cm^{-1} for the transitions $4p$-$3d$ at 2177 Å and $4s$-$3p$ at 1894 Å, respectively. The $4f$-$3d$ transition has an oscillator strength about one. Therefore, it offers higher gain than the other 4-3 transitions. The calculated peak gain is 0.34 cm^{-1} for the transition $4f$-$3d$ at 2163 Å. The gain conditions of the $4f$-$3d$ transition are different from those of the $4p$-$3d$ transitions due to the fast radiative decay of the transition $4f$-$3d$. It changes more rapidly with changing N_e than the other transitions.

So far we have neglected the effects of opacity on the gain. At $N_e \sim 5\times10^{15}$ cm^{-3} and $T_e=4$ eV, the line-center absorption coefficient is 1.5 cm^{-1} for the transition $3d$-$2p$ at 574 Å. Optical trapping in the strong transitions of 3-2 can reduce the 4-3 population inversions by increasing the $n=3$ level populations well above their optically thin values although the enhanced $n=4$ populations are not much influenced by optical trapping. For a 1.0-cm optical-path length and $T_e=4$ eV, the calculated gain including trapping of the 4-3 transitions versus electron density is shown in Fig. 7. In the optically thin case, the ratio of peak gain at the 2177- and 2163-Å lines is about 2.5. Since the spontaneous decay rate of the $4f$-$3d$ transition is about 14 times that of the $4p$-$3d$ transition, opacity affects $4f$-$3d$ gain more. A 30% reduction of gain occurs for C III at 2177 Å, and a 70% gain reduction occurs for C III at 2163 Å due to opacity. In Fig. 7 the peak gains of the $4f$-$3d$ and the $4p$-$3d$ transitions are 0.09 and 0.10 cm^{-1}, respectively. These values are considerably lower than those for the optically thin calculation.

The question still remains as to what equilibrium population distribution is reached due to photoexcitation and in what time interval? To determine this one must examine the relaxation time and the perturbation of the ground-state density due to photopumping. For the 20-eV brightness temperature of the pump-line intensity, the population ratio of the ground state to enhanced $4p$ level is less than 100. Less than 5% of the electrons in the ground state are being pumped to the upper $n=4$ levels. This slight change of the ground-state population means that the perturbation of the ground state can be ignored. Furthermore, the populations of excited states arrive at equilibrium with the ground states in times on the order of 1 ns. If the time of variation of the intensity of the pumping radiation is greater than 1 ns, which is the case as shown in the experiments, the local excited-level populations can be assumed to achieve quasi-steady-state values with respect to a given ground-state density n_{2s},

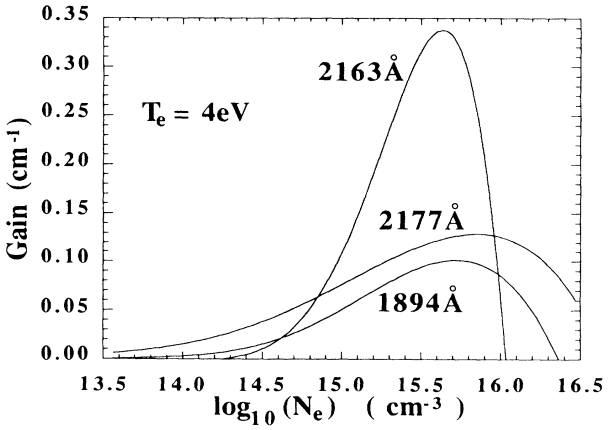

FIG. 6. Calculated gain vs electron density at $T_e=4$ eV without phototrapping.

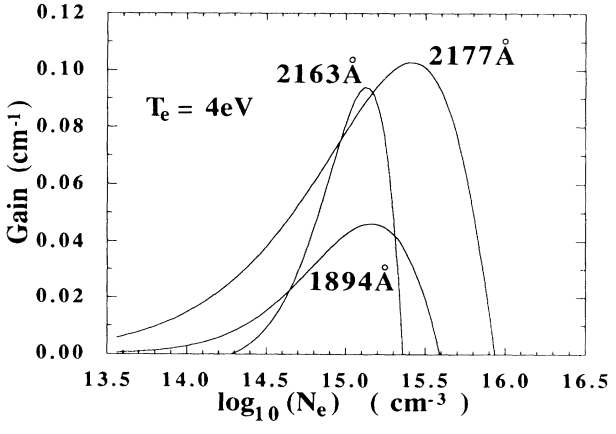

FIG. 7. Calculated gain vs electron density at $T_e=4$ eV assigning a 1.0-cm optical-path length.

electron density N_e, electron temperature T_e, and pumping strength $P(T_{\mathrm{Mn}})$. Therefore fluorescence due to pumping is expected to follow in time the intensity of the pump Mn VI–line radiation.

The above analysis shows that the C III plasma should have a density of 3×10^{15} cm^{-3} and a temperature of 4 eV to maximize gain. The Mn plasma, on the other hand, should have higher densities and temperatures ($\sim$20 eV). These disparate requirements demand separate plasmas. The carbon plasma was produced in a vacuum arc, and the Mn ions in a laser-produced Mn plasma. For a vacuum-arc discharge with currents of about 10 kA, electron density can range from 10^{13} to 10^{16} cm^{-3}, and electron temperature usually is a few eV. In a laser-produced plasma, N_e is from 10^{17} to 10^{21} cm^{-3} and T_e is from 10 to 100 eV. Over such a range of plasma conditions, the model of the C III–Mn VI laser scheme was examined. The calculations indicate that a small signal gain of 0.1 cm^{-1} is obtainable in C III at 2177 and 2163 Å using resonant photoexcitation. Cavity losses near the 2170-Å wavelength region are about 20% using available mirrors. Lasing is thus possible at 2177 and 2163 Å in C III. The measurements of electron density N_e and electron temperature T_e in the plasmas are described in the next section. These early experiments led to further experiments in which fluorescence, small-signal gain, and eventually laser oscillation on 4-3 transitions in C III, were all measured.

III. OPTICAL SPECTROSCOPY STUDY OF THE C PLASMA

The detailed atomic physics code described above had pointed to specific line-intensity measurements, which would give reliable values of N_e and T_e. These measurements are described in detail below. Figure 8 shows the experimental apparatus. The carbon plasma was produced in a vacuum-arc discharge between a hollow carbon anode and a 6-mm-diam solid-C cathode as shown. The interelectrode separation is 100 mm. The discharge was driven by an L-C ladder network consisting of 11 8.5-μF capacitors with 1-μH station to station inductors. The network was charged typically to -6 kV. The high voltage was applied to the cathode in series with a 1.0-Ω $CuSO_4$ resistor. The resistance of the vacuum-arc discharge is typically 40 mΩ, so the $CuSO_4$ resistor served as the matching impedance for the ladder network. A discharge was triggered by focusing a (15 J)/(70 ns) CO_2 laser onto the cathode surface. The resulting discharge current exhibits a 20-μs rise time, 50-μs flat-topped duration, with a current of $\sim$6 kA at 6 kV. The carbon plasma was viewed by the 0.2-m, the 2-m Ebert, and the Jarrel-Ash spectrometers at right angles to the discharge axis and at five positions downstream from the C cathode. The plasma region ($\sim$2 mm$\times$15 μm) on the discharge axis was imaged onto the spectrometers. A one-to-one imaging system was chosen for the 2-m spectrometer by using two identical lenses, each of which was 2 in. in diameter and 20 in. in focal length. The 2-m Ebert monochromator offered sufficient resolution to observe a specific narrow portion of the emitted spectral line to be scanned. The scanning was accomplished by repeated firings of the C discharge while advancing the instrument in wavelength steps. To ensure that the true spectral linewidth is measured accurately, narrow entrance and exit slits ($\sim$15 μm) were used for the 2-m spectrometer and higher orders of the spectral lines were studied. The instrumental widths were measured by scanning the narrow lasing line of Ne I at 6328 Å and the Hg I line at 4046.6 Å. A Gaussian function was found to be a good representation of the instrumental slit profiles, and the FWHM was found to be 0.2 Å in first order for the 2-m spectrometer. This Gaussian representation was then used for any necessary deconvolution of instrumental widths. The 0.2-m spectrometer, which was calibrated with its imaging system, was used to measure the absolute line intensity. Figure 9(a) shows the discharge current as a function of time. Figures 9(b), 9(c), and 9(d) show the detected line intensities of a C II line at 2993 Å and C III lines at 4647 and 3609 Å, respectively. When the discharge current reached the flat-topped portion, the emission signal was steady, which suggests that the plasma conditions were quasisteady. The line intensity was measured at the time when the current waveform was flat. Three shots were taken at each wavelength or line. In shot-to-shot scanning of line shapes and measuring the absolute line intensity, the Jarrel-Ash monochromator was used to measure the integrated C III–line intensity at 5696 Å, as a monitor. The reproducibility was adequate, i.e., data were taken only when the 5696-Å intensity remained constant over many shots.

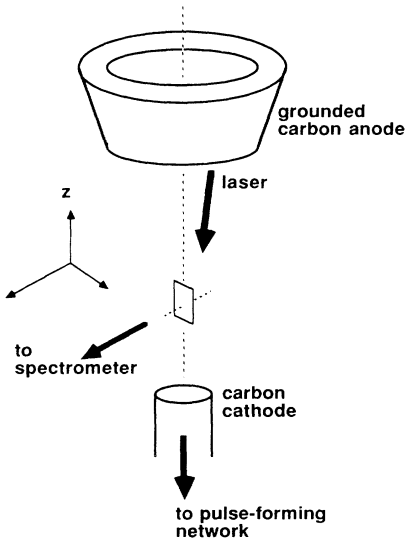

FIG. 8. Schematic diagram of experimental apparatus of the electron density and temperature measurements.

Figure 10 is a partial Grotrian diagram of carbon ions. The electron temperature and density can be obtained from the ratio of the C III 4647-Å to the C III 3609-Å line intensities and from absolute line intensities of these lines. Doppler-broadened line profiles of the C III $3p\ ^3P^\circ$–$3s\ ^3S$ at 4647-, 4650-, and 4651-Å wavelengths were measured, from which were inferred ion temperatures in the C plasma. Scanning Stark-broadened line profiles of the C II

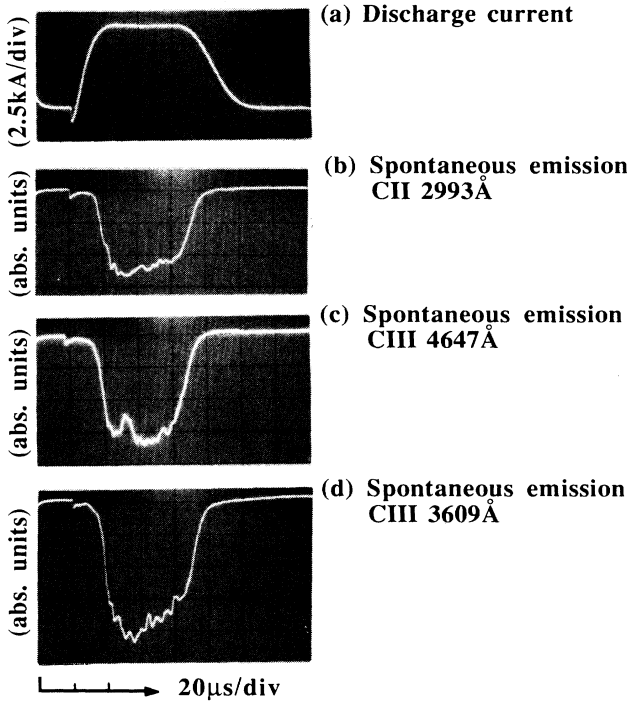

FIG. 9. Line intensities of carbon ions vs time.

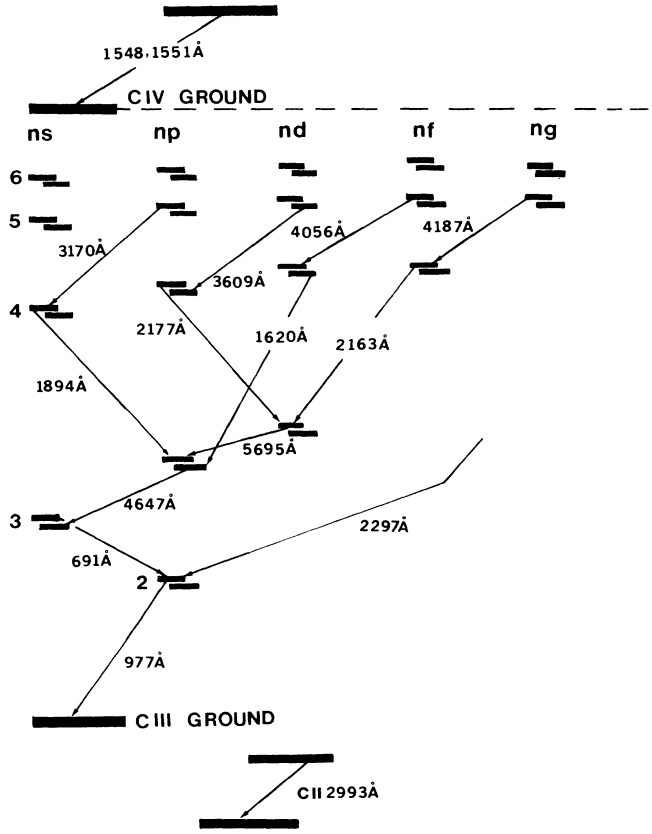

FIG. 10. Partial Grotrian diagram of carbon ions.

line at 2993 Å and the C III $5d\,^3D-4p\,3P^\circ$ lines at 3608.8-, 3609.1-, and 3609.6-Å wavelengths provided electron densities. The measured data were fit by Gaussian or Lorentzian line profiles. Parameters in the line profile, such as the FWHM and the background of continuum radiation, were varied until the best fit was obtained. To ensure that these lines were optically thin, the optical depths of these lines were examined. The experimental arrangement for these measurements was to add an imaging system. This system reflected the line emission along the 2-m spectrometer axis back to its origin. If any absorption occurred, the line profiles with and without reflection would be different, because there would be more absorption at the center of the line than at the wings. It was found that all these lines were optically thin, except the C III line at 2297 Å.

The experimental results and the analysis follow.

A. C III, $3p\,^3P^\circ-3s\,^3S$ transitions

Figure 11 shows a typical measured line profile fitted by a Gaussian function. When the 4647.42-Å intensity is set to 100, the measured intensity is 70 at 4650.4 Å and 25 at 4651.5 Å. These intensities are consistent with spin-orbit- (LS) coupling theory,[53] which is a good approximation in light ions such as carbon. The measured relative line intensities are very close to those from LS coupling, which also implies that self-absorption of these lines is negligible.

The line profiles were measured by using the second order of these spectral lines so that the instrumental FWHM was reduced to 0.1 Å. Stark widths of these lines[54] could be ignored compared to the measured linewidths. A sample of a measured line profile, fitted by a Gaussian function, is shown in Fig. 12. In Fig. 12, the

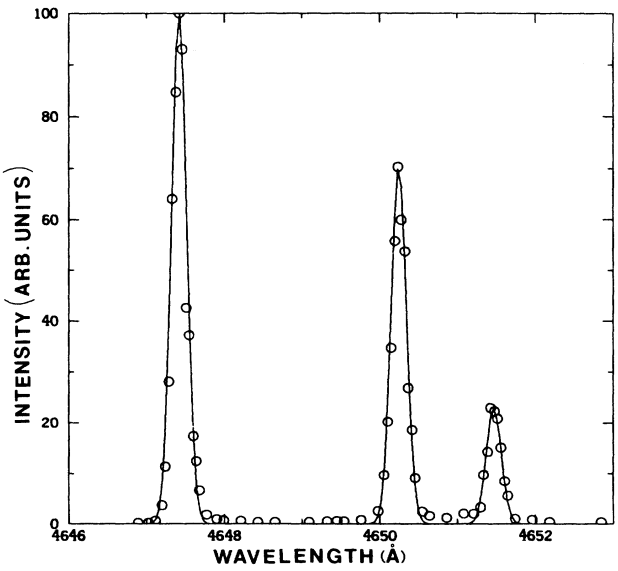

FIG. 11. Observed C III $3p\,^3P^\circ-3s\,^3S$ multiplet transition profiles at 4647.4, 4650.4, and 4651.5 Å. The line profiles were fit well by a Gaussian function.

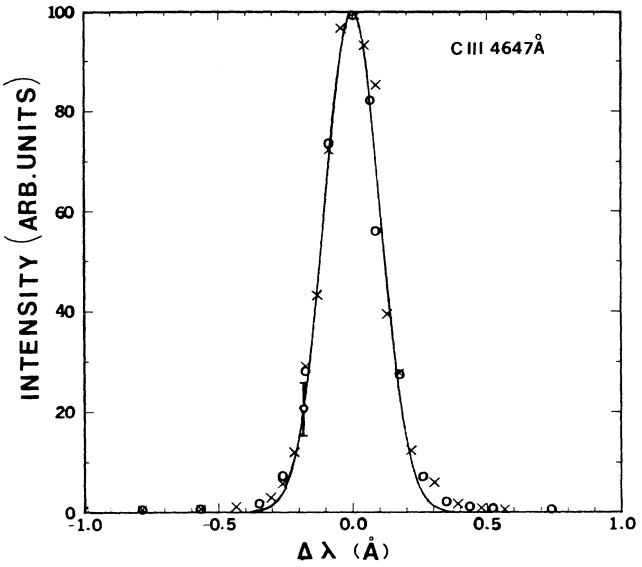

FIG. 12. Measured Doppler-broadened line profile of C III 4647 Å. The open circles and the crosses are the experimental data points without and with the back reflection, respectively.

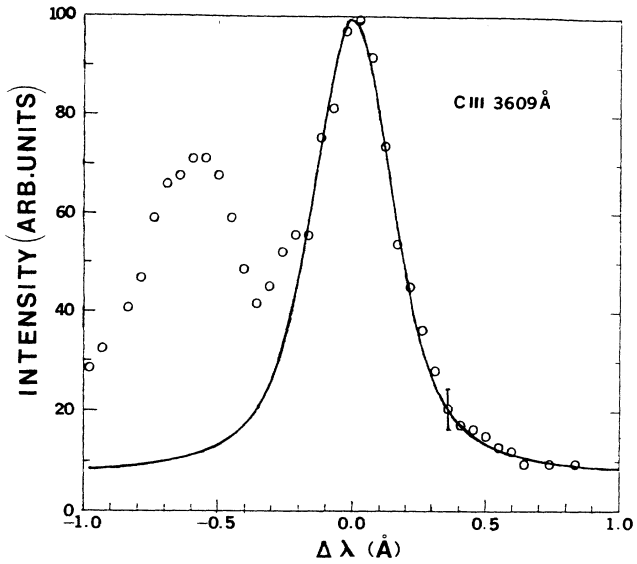

FIG. 13. Measured Stark-broadened line profile of C III 3609 Å. The open circles are the experimental data points.

crosses and circles are the normalized experimental data points with and without the back reflection, respectively. The best-fit Gaussian has a FWHM of 0.30 Å. Doppler broadening may also be caused by gross mass motion in the C discharge. The estimated radial velocity V_r of the C ions is

$$V_r \sim V_s \frac{R}{L} = 1.5 \times 10^5 \text{ cm/s} , \tag{8}$$

where V_s is the ion velocity ($\sim 10^6$ cm/s) downstream along the C-discharge axis, R (=15 mm) is the diameter of the C anode, and L (=100 mm) is the separation of the C electrodes. This motion gave an uncertainty of about 0.02 Å to the linewidth. The derived ion temperatures are within an estimated error of 15% due to the fluctuation of the C plasma and the streaming motion of the ions.

B. C II 2993-Å and C III $5d\ ^3D - 4p\ ^3P^\circ$ transitions

The measured line intensities of the C III $5d\ ^3D - 4p\ ^3P^\circ$ multiplet transition are 100:65:15. These values are similar to those predicted by *LS*-coupling theory. Since the widths of these lines ($5d$-$4p$ transitions in C III) are the same as measured, the line profile of the strongest transition at 3609.6 Å in C III was used in the analysis. By using the third order of the C III 3609.6-Å and C II 2993-Å lines, the instrumental width was reduced to 0.07 Å. At lower electron densities Doppler broadening tends to be comparable with Stark broadening. The so-called Voigt function[55] was used to convolute such profiles. Typical measured line profiles at 3609.6 Å in C III and at 2993 Å in C II are shown in Figs. 13 and 14, respectively. Figure 13 shows a best fit of a Lorentzian profile to the C II line at 2993 Å with FWHM of 0.55 Å. The crosses and the circles are measured data points, which correspond to measurements with and without the back reflection, respectively. Figure 14 shows a typical measured profile of the C III-line fit by a Voigt profile at 3609.6 Å, obtained at 8.0-kA discharge current. The Stark width was not reliable from the C III 3609-Å line at the 4.4-kA discharge current due to the dominant Doppler width or from the C II 2993-Å line at 8.0-kA discharge current due to opacity effects. Electron density was derived from the full Stark width $\Delta\lambda_S$ measured in (Refs. 56–58) Å by

$$N_e = b[\Delta\lambda_S(\text{in Å})] \times 10^{16} \text{ cm}^{-3} , \tag{9}$$

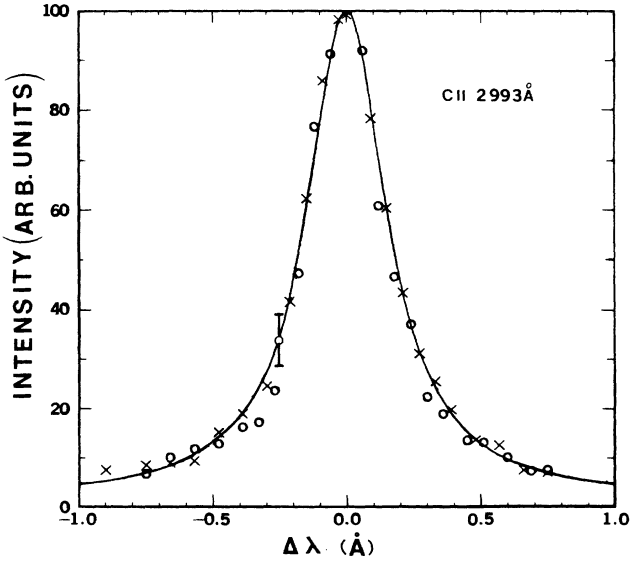

FIG. 14. Measured Stark-broadened line profile of C III 2993 Å. The open circles and the crosses are the experimental data points without and with the back reflection, respectively.

where b is 0.25 for the C II line at 2993 Å and 6.45 for the C III line at 3609 Å.

C. C III $2s2p\ ^1P^\circ - 2p^2\ ^1D$ at 2297 Å

This line is found to be optically thick from the line-profile measurements. An optically thick line profile can be written as

$$I(\Delta\lambda)=I_0(\Delta\lambda)[1-\exp(-kl)]\ , \tag{10}$$

where l is the optical-path length, $I_0(\Delta\lambda)$ is the line profile without opacity, and k is the absorption coefficient defined by

$$k(\Delta\lambda)=(2.74\times10^{-11})An\frac{\alpha}{\Delta\lambda_D}\times\int_{-\infty}^{\infty}\frac{\exp(-y^2)}{(\beta-y)^2+\alpha^2}dy\ \text{cm}^{-1}\ , \tag{11}$$

where A is the transition probability,[59] n is the density of the $2s2p$ state, $\alpha=0.833\Delta\lambda_S/\Delta\lambda_D$ and $\beta=0.833\Delta\lambda/\Delta\lambda_D$. By using electron densities and ion temperatures measured from C III and C II linewidths, the Doppler width $\Delta\lambda_D$ and Stark widths $\Delta\lambda_S$ of the line were determined, where the Stark width $\Delta\lambda_S$ is given[58] by

$$\Delta\lambda_S=3.4\times10^{-18}N_e(\text{in cm}^{-3})\ \text{Å}\ . \tag{12}$$

The optical-path length l was estimated by using the Jarrel-Ash spectrometer to measure the emission of the C III 5696-Å line radially across the C-discharge axis. The measured optical-path length l was about 1.0 cm along the 2-m spectrometer axis. To measure the line profile more accurately, the fourth order of the spectral line was used, as the line was very bright. Figure 15 presents a typical measured line profile fitted by Eq. (10) with an optical depth kl of 4 at line center (solid line), while the dashed line is the optically thin line profile. The population n of the lower transition level (first excited state) $2s2p$ of the C III 2297-Å line was obtained by fitting the optical depth of this line. Knowing n and N_e, the electron temperature T_e was derived from the code. The absolute line intensities of the C III 2297-Å line where also measured by using the 0.2-m spectrometer. The line profiles acquired a flat top about the line center (see Fig. 15). This flat top is at an intensity level equal to that of a blackbody radiating thermally at the temperature of the C plasma. The resolution of the 0.2-m spectrometer is greater than the linewidth. By using the measured line and instrumental profiles, the absolute intensity at the line center was deduced from the measured total line intensity. The derived electron temperatures from this measurement ware within 15% of those obtained from the measured optical depth.

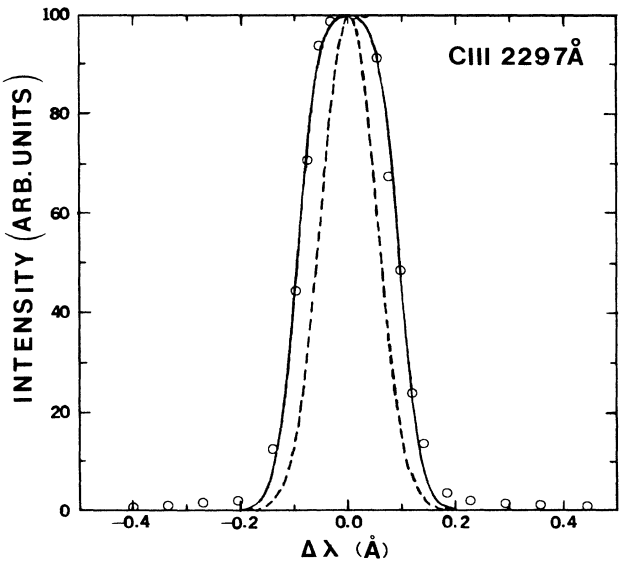

FIG. 15. Measured profile of the optical thick line C III 2297 Å. The solid line is the best fit with FWHM 0.12 Å and optical depth $kl=4$. The dashed line is the line profile in the optically thin case.

Furthermore, the absolute line intensities of C III at the 4647- and 3609-Å wavelengths were measured. The ratio of these two line intensities was used to infer the electron temperature in the emitting region, while the absolute intensities gave the populations of the excited states, which were used to infer the electron densities in the plasma. These results are consistent with those from the line-profile and line-intensity measurements.

The results of the measured plasma density and temperature are shown in Figs. 16 and 17, respectively. Figure 16 shows the measured electron density as a function of Z, the distance downstream from the C cathode, at several discharge currents. Figure 17 shows the measured ion and electron temperatures versus Z. The electron densities are about 5×10^5 cm^{-3} and electron temperature about 4 eV at 6.4-kA discharge current. Such plasma conditions were chosen for the photoexcitation experiments.

In summary, measurements of electron densities and temperatures in the C discharge have been described. For the resonant photoexcitation experiment the pump source is a laser-produced Mn plasma. A brightness tem-

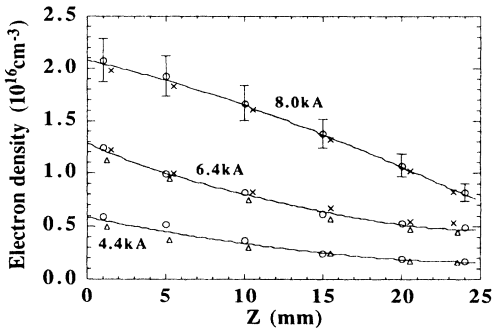

FIG. 16. Measured electron density along the C-discharge axis as a function of Z, downstream from the C cathode surface. ×, experimental data points measured from the Stark width of C III line at 3609 Å; △, experimental data points measured from the Stark width of C II line at 2993 Å; ○, experimental data points measured from the absolute line intensities of C III lines at 4647 and 3609 Å.

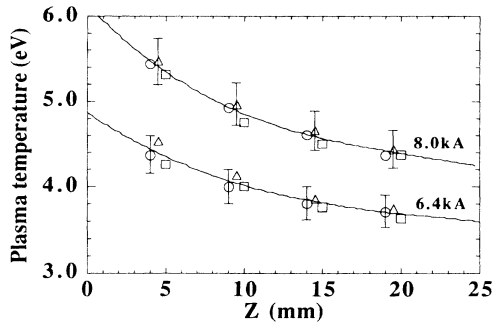

FIG. 17. Measured plasma temperature along the C-discharge axis as a function of Z, downstream from the C cathode surface. ○, ion temperature obtained from the Doppler width of C III 4647-Å line; ×, electron temperature obtained from the line ratio of the C III 4647-Å to C III 3609-Å; △, electron temperature from the absolute line intensities of C III lines at 2297 and 4647 Å.

perature of 20 eV for the Mn VI–pump-line radiation was estimated by measuring the absolute continuum intensity from the Mn plasma and by using a hydrodynamic and kinetic model of the laser-produced plasma. With these measurements, the proper plasma conditions can be estimated for obtaining population inversions. The fluorescence and gain obtained due to such population inversions are presented in Sec. IV.

IV. FLUORESCENCE, GAIN, AND LASER OSCILLATION AT 2177 AND 2163 Å IN C III

Figure 18 is a schematic drawing of the experimental apparatus used for the gain and lasing measurements. The C III plasma is produced in a vacuum discharge as described in Sec. III. The axis of the C discharge is turned 90° such that it is in the same plane as the axes of the spectrometers. The C cathode is located 5 mm off the optical axis of the 0.2-m spectrometer, which is used to measure fluorescence and gain on the C III $n=4$ to $n=3$ transition lines. The hollow C anode is placed on the spectrometer axis. The axis of the C discharge is not coincident with the spectrometer axis. The electron density is about 5×10^{15} cm^{-3} and the temperature about 4 eV, on the spectrometer axis at a 6.4-kA discharge current. The discharge plasma so produced consists mostly of C III ions, as measured and calculated by the CR model. The Mn pump plasma is produced by focusing another (10 J)/(70 ns) CO_2 laser to a 2×23 mm^2 line focus on a Mn slab as shown. The line focus is parallel to the 0.2-m spectrometer axis and is 7 mm away from it. Typically, the Mn laser-produced is produced 36 μs after discharge initiation. Enhanced fluorescence coincident with the Mn plasma was observed on many 4-3 transitions in C III. Figure 19 shows typical enhanced fluorescence measurements at 2177 Å in C III. Figure 19(a) shows the 6.4-kA peak, discharge current versus time. The first "noise" fiducial (10 μs into the sweep) on Fig. 19(a) shows when the first laser is fired to trigger the C discharge. The later "noise" fiducial shows that the second laser is fired 36 μs after the first. Figure 19(b) shows the spontaneous emission on the C III $4p$-$3d$ line at 2177 Å. The trace shown is an average over five successive discharges. Figure 19(c) shows the enhanced fluorescence at 2177 Å, when the Mn laser-produced plasma was created, 36 μs after discharge initiation. To capture this enhanced fluorescence, the sensitivity of the detecting electronics was decreased by a factor of 45. To be sure that the enhanced fluorescence came from the C III ions, the Mn plasma was created without the C discharge. In this case, Fig. 19(d) shows that there was some small spurious background radiation at 2177 Å from the Mn plasma. When this background was subtracted from the fluorescence in Fig. 19(b), the net enhanced fluorescence was 170 times the spontaneous emission, which was very close to the prediction of 160 from the CR model. Such enhancements were found to be very reproducible from shot to shot. The typical duration of the enhanced fluorescence (FWHM) was about 0.3 μs. This is consistent with the prediction of a self-similar

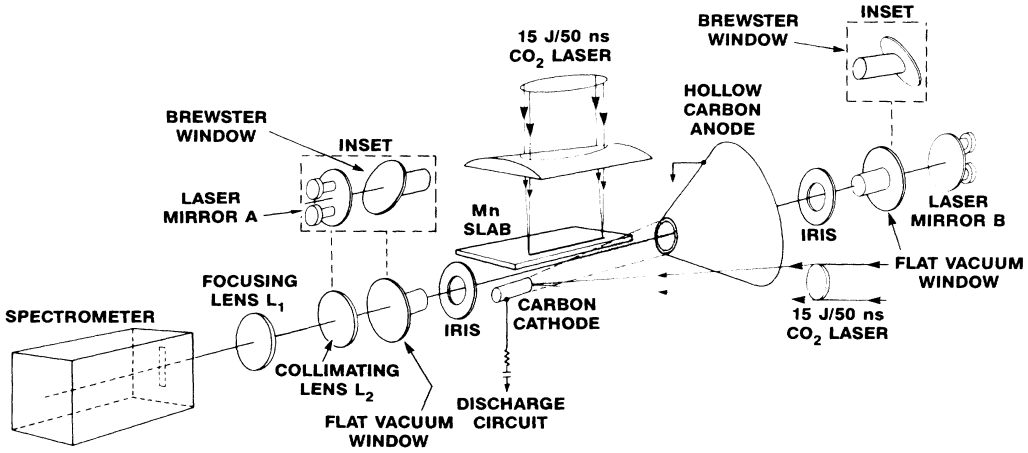

FIG. 18. Schematic diagram of the experimental apparatus.

hydrodynamic code for the Mn plasma expansion,[52] which estimated that the Mn VI–pump-like radiation had about a 0.3-μs pulse duration.

Similar measurements were then made at several other $n=4$ to $n=3$ transitions in C III. The net enhanced fluorescence on the $4s\ ^1S-3p\ ^1P^\circ$ line at 1894.5 Å, and the $4f\ ^1F^\circ-3d\ ^1D$ line at 2163 Å was found to be approximately a factor of 70 above the spontaneous emission. Enhanced fluorescence was also measured on the $4d\ ^3D-3p\ ^3P^\circ$ line at 1620 Å and the $4f\ ^3F^\circ-3d\ ^3D$ line at 1923 Å. Typical results are shown in Figs. 20–22. In Figs. 20–22, (a) shows the spontaneous emission at C III 2163, 1894, and 1923 Å, respectively; (b) shows the fluorescence due to photoexcitation and collisional transfer at these lines; (c) is the background due to the laser-produced Mn plasma alone (C discharge off) at these wavelengths. These measurements confirmed that the selective photoexcited population of the $4p\ ^1P^\circ$ state is accompanied by rapid collisional exchange of this population with other $n=4$ levels. The ratio of the net fluorescence to the spontaneous emission agreed well with the calculation of the collisional-radiative model, which predicted a ratio of 100 at 1894 Å and 90 at 2163 Å for the C III lines.

As shown above, fluorescence was observed on many 4-3 transitions in C III. It might be argued that the ob-

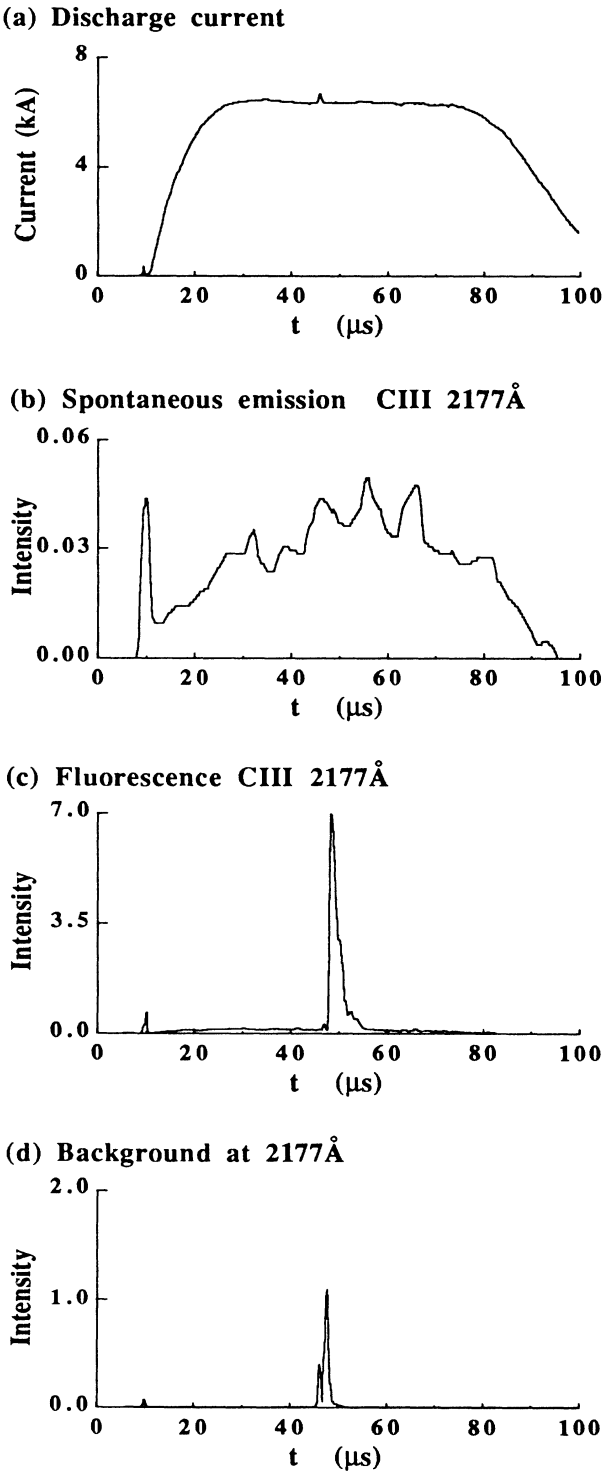

FIG. 19. Observed fluorescence at 2177 Å in C III. Radiation emission intensities are in arbitrary units.

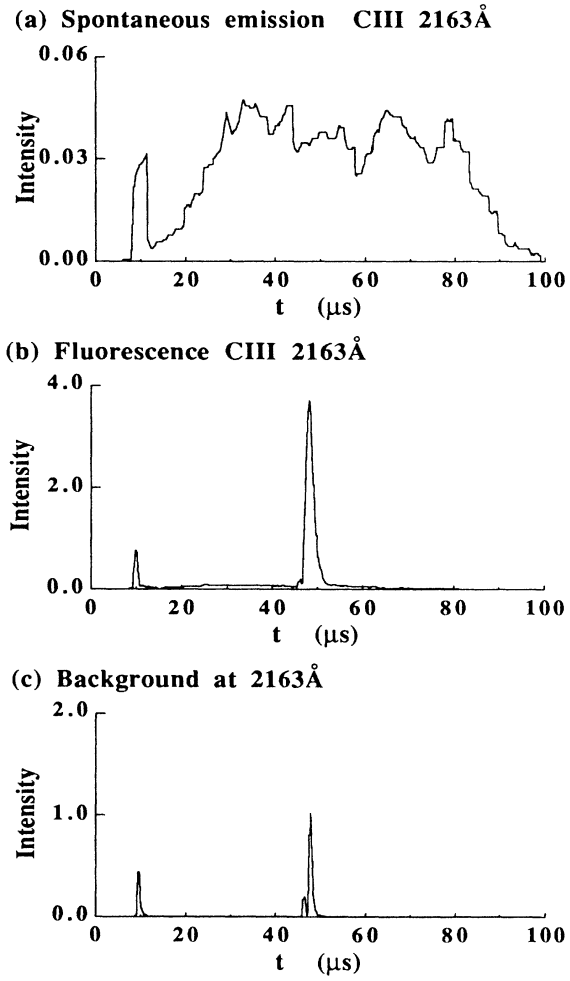

FIG. 20. Observed fluorescence at 2163 Å in C III. Radiation emission intensities are in arbitrary units.

served fluorescence was due not to a resonant excitation, but due to collisional excitation in C III by the hot electrons from the laser-produced Mn plasma which expanded into the C discharge, or was due to broadband photoionization and collisional ionization of C III ground-state ions, which then recombined and cascaded down from high levels to $n=2$ levels. To test these alternative hypotheses, the Mn plasma was replaced by a laser-produced Al plasma. Since there were no coincident transitions between Al and C III ions, no resonant photoexcitation was expected. However, the Al plasma should be similar to the Mn plasma in other respects, and hence should show the same nonresonant effects. The experiment showed no fluorescence observed on the 4-3 transitions with the Al plasma. As a further check, resonance lines of C II at 1335 Å, C III at 977 Å, and C IV at 1548 Å were examined in the presence of a Mn plasma. The upper states of these lines were coupled to the ground states by strong dipole transitions, and would reveal an increase in the ground-state populations, if broadband photoionization occurred. Under conditions similar to those described earlier, the emission at these wavelengths was measured in the C discharge with laser-produced Mn or Al plasmas. No fluorescence was observed at these wavelengths. These measurements together serve to confirm the selective photoexcitation of C III due to Mn VI–line radiation.

To summarize the fluorescence measurements, let us compare the *net* fluorescence measured on each of the C III 4-3 lines with the predictions of the atomic model, for chosen values of $N_e=10^{16}$ cm^{-3} and $T_e=4$ eV. Table I shows the comparison. The agreement is remarkably good and motivates the search for gain, which was the next step.

To measure gain, a mirror was added to the spectrometer axis, as shown in Fig. 18. The mirror, placed behind the hollow anode, was adjusted to reflect rays from the midregion of the C III plasma back through the plasma. Irises were placed on either side of the discharge, to ensure that the solid angles subtended by the mirror and the spectrometer gathering optics were identical. On successive shots, the spontaneous emission and enhanced

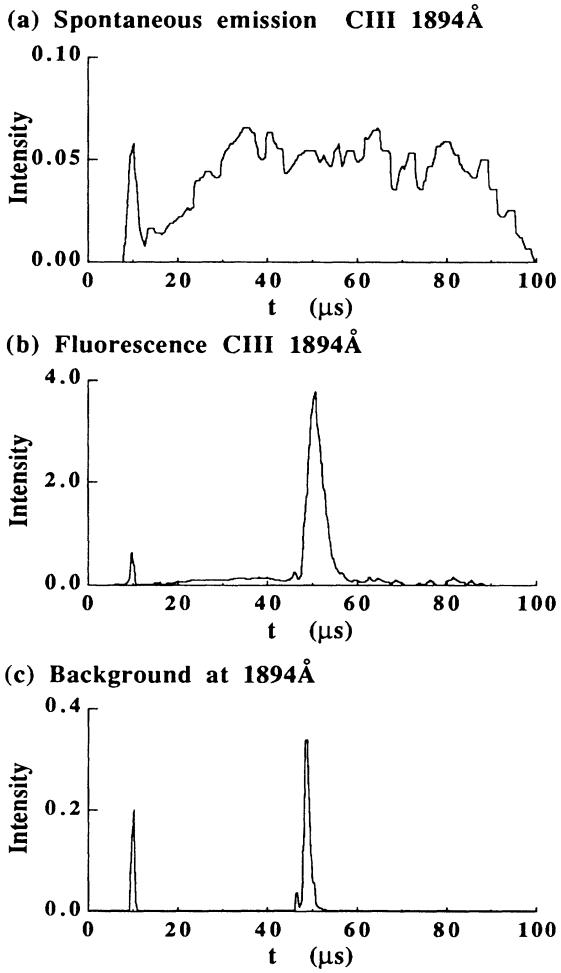

FIG. 21. Observed fluorescence at 1894 Å in C III. Radiation emission intensities are in arbitrary units.

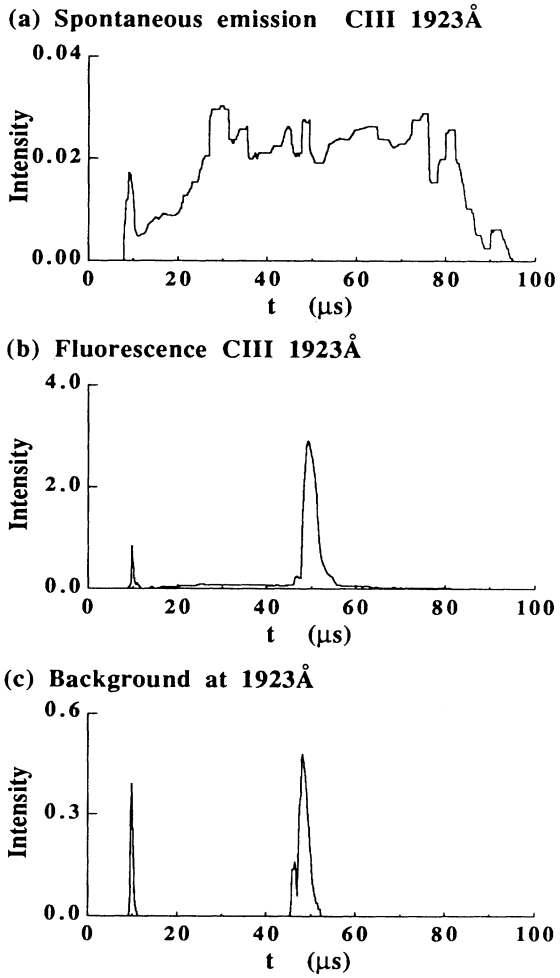

FIG. 22. Observed fluorescence at 1923 Å in C III. Radiation emission intensities are in arbitrary units.

TABLE I. Ratio of fluorescence to spontaneous emission.

Wavelength (Å)	Transition	Experiment	Calculated
2177	$4p$-$3d$	170	160
2163	$4f$-$3d$	70	90
1894	$4s$-$3p$	70	65

fluorescence were measured with and without the mirror. The ratio R of the measured line intensities with and without the mirror is given by

$$R = 1 + rt^2 \exp(G) , \tag{13}$$

where r is the reflectivity of the mirror, t is the transmittance of the vacuum window, and G is the integrated gain coefficient along the entire optical-path length (~ 2 cm). For noninverted optically thin lines, $G=0$, hence $R = 1 + rt^2$. For an inverted transition with gain, $G > 0$ and $R > 1 + rt^2$.

The line chosen for calibration of this technique is the C II line at 2174 Å. This line was measured to be optically thin and known to be unaffected by the photoexcitation of C III. Also, this line is very close in wavelength to the C III 2177- and 2163-Å lines on which gain was measured. Figure 23 shows the results of the calibration experiments. Figure 23(a) shows the C II 2174-Å spontaneous emission versus time, without the mirror. At $t=36$ μs, there appears to be some enhanced fluorescence due to the Mn laser-produced plasma. However, Fig. 23(c) shows the spurious background detected at 2174 Å, due to the Mn plasma alone. When this background is subtracted from the emission signal in Fig. 23(a), it is clear that the 2174-Å C II line is unaffected by optical pumping. Figure 23(b) shows the C II 2174-Å line emission with the reflecting mirror. The ratio R of the average spontaneous emission in Fig. 23(b) to that in Fig. 23(a) was 1.5 ± 0.15, i.e., $r = 0.5 \pm 0.15$. The ratio of the spurious background due to the Mn plasma, with and without the mirror, is also about 1.5. The ratio R for the spontaneous emission on the C III line at 2163 Å was also measured and R was found to be 1.5 ± 0.1.

Figure 24 shows the measurement of R at 2177 and 2163 Å in C III with the Mn VI–pump-line radiation, and evidence for gain. Figure 24(a) shows the enhanced fluorescence at 2177 Å, without the reflecting mirror. The spontaneous emission was a factor of 170 smaller than this enhanced fluorescence, and so was buried in the baseline. Figure 24(b) shows the fluorescence with the reflecting mirror. The ratio of R was 2.1 ± 0.1. For measured $r = 0.5 \pm 0.1$, this gives $G = 0.8 \pm 0.3$. For a 2-cm effective-gain length in the C III plasma, the measured gain coefficient was 0.4 ± 0.15 per cm. Figures 24(c) and 24(d) show similar results on the C III line at 2163-Å wavelength. For this line too, R was found to be 2.1 ± 0.1 and the gain coefficient was 0.4 ± 0.15 cm^{-1}. At both

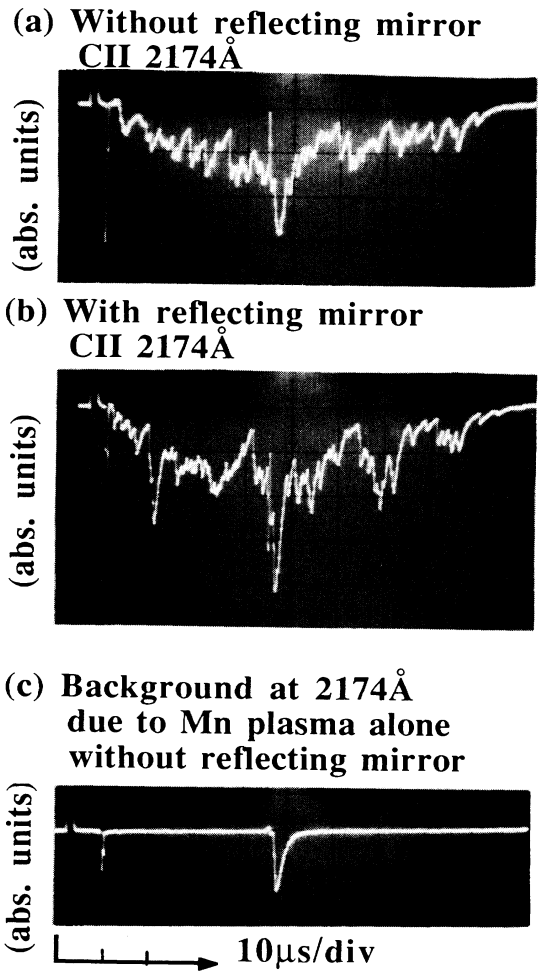

FIG. 23. Calibration experiment for single-pass gain measurement. (a) and (b) are spontaneous emission at 2174 Å in C II detected without and with the reflecting mirror, respectively. (c) Spurious background at 2177 Å due to the laser-produced Mn plasma alone.

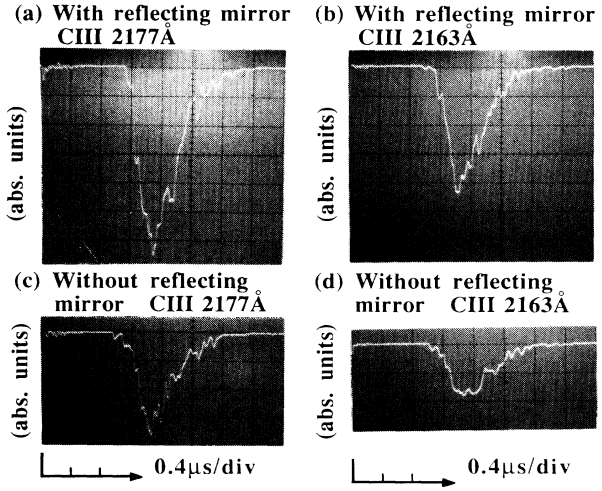

FIG. 24. Single-pass gain at 2177 and 2163 Å in C III. (a) and (c) are enhanced fluorescence, with the reflecting mirror, at 2177 and 2163 Å, respectively. (b) and (d) are enhanced fluorescence, without the reflecting mirror, at 2177 and 2163 Å, respectively.

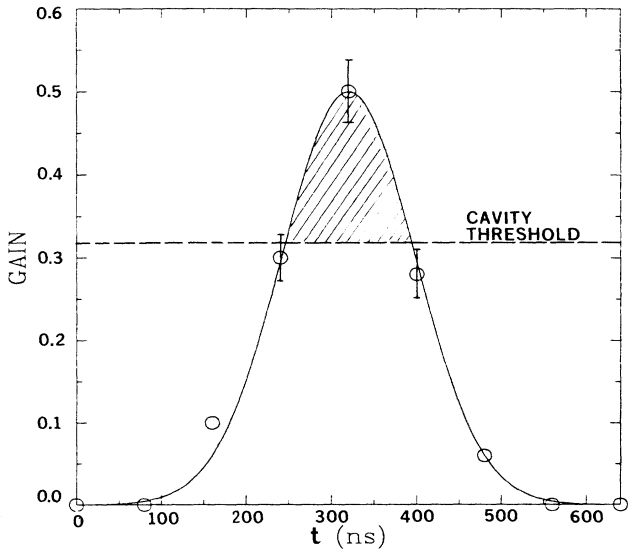

FIG. 25. Single-pass gain-length product vs time, for C III, 2177- and 2163-Å lines. The dashed horizontal line is the cavity loss threshold of 0.30. Net gain occurs in the shaded region.

2163 and 2177 Å the measured values of R versus time were within ±20% of each other and R was 1.5 (implying gain), for about 0.3 μs. A representative plot of the single-pass, gain-length product (G) versus time is shown in Fig. 25. The values of G shown in Fig. 25 are similar to the predictions of the collisional-radiative model, but the measured gain coefficients are higher than those predicted by the model. The discrepancy can be due to the uncertainty in transition probabilities, opacity broadening of the pump line, and overestimation of the effects of opacity in the C discharge. The wavelength-mismatch effect between the pump and the pumped line can be reduced if the Mn VI pump line is optically thick. As a result, the photopumping is more effective than was assumed in the model so that the gain is increased. Streaming motion of the C ions, smaller lateral plasma dimension than that assumed, and the effect of gradients will all reduce the opacity effects and correspondingly increase the predicted gains.

To seek laser oscillation at 2177 and 2163 Å, a Fabry-Perot confocal resonator was used. (See inset in Fig. 18 or Fig. 2 in Ref. 60.) The two mirrors had a 1-m radius of curvature and a (1.995±0.004)-m separation (for stability). The reflectivity, r=92%, of the two mirrors at the two laser wavelengths was measured using a photometer. Also, the vacuum windows were replaced by fused-silica Brewster windows. The transmittance of these windows began at 96% but decreased to ~90% after just a few discharges. After tens of discharges, the transmittance had decreased to ~80%. The decrease was caused by deposition of carbon from the discharge on the vacuum side of the Brewster windows. The cavity threshold, $-\ln(rt^2)$, where r (=92%) is the reflectivity of the laser mirrors, thus increased from 0.165 to 0.53 during a typical experiment, before the Brewster windows were replaced. Since a few discharge shots had always occurred before any multipass amplification measurements were made, it is assumed that the cavity threshold was ~0.30 (90% transmission of the Brewster window) for the results in the measurements. This mean threshold is shown as a horizontal dashed line in Fig. 25. The net gain-length product (per pass) is the portion of the gain curve (shown shaded) which is above the threshold. Summation of the net gain-length product per pass over 50 passes gives a total (cavity) gain-length product of ~4.5.

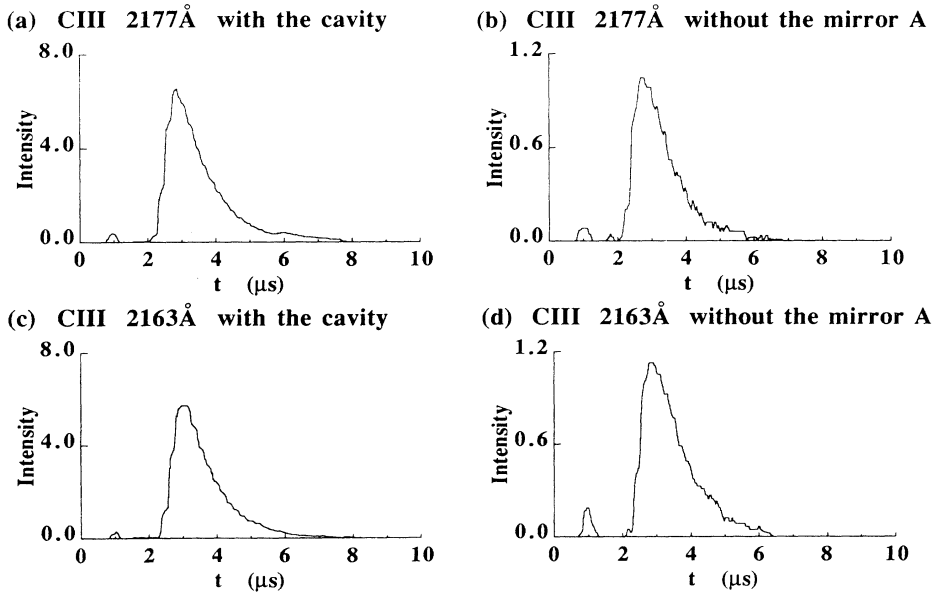

FIG. 26. Evidence for lasing in C III. (a) and (c) are emission, with the laser cavity, at 2177 and 2163 Å, respectively. (b) and (d) are emission, with the front mirror A removed, at 2177 and 2163 Å, respectively. Radiation emission intensities are in arbitrary units.

Neglecting gain saturation, this implies that stimulated emission was amplified by a factor of exp(4.5)=90. To detect this enhancement, the ratio of the line intensity with and without the front mirror A of the laser cavity was measured. Typical results are shown in Fig. 26. Figures 26(a) and 26(c) show the intensities with the tuned cavity at 2177 and 2163 Å, respectively. Figures 26(b) and 26(d) show the intensities with the front mirror A removed. The signals in Figs. 26(b) and 26(d) correspond to a single pass of amplification, whereas the signals in Figs. 26(a) and 26(c) correspond to ~ 50 passes of amplification, and should therefore be greater. The ratio of these two signals inside the cavity should be $\sim \exp(4.5)/\exp(0.1) \sim 80$. However, because the front mirror A transmits only 8%, the ratio at the detector should be ~ 6, i.e., the signal with the front mirror A removed should be six times lower than that with the tuned cavity. It is assumed in these estimates that the solid angle for detection of the two signals is the same. This was ensured in the experiment by placing a pair of irises 500 mm apart along the optical axis. The signals in Figs. 26(a) and 26(c) are about five to six times greater than those in Figs. 26(b) and 26(d), confirming laser oscillation.

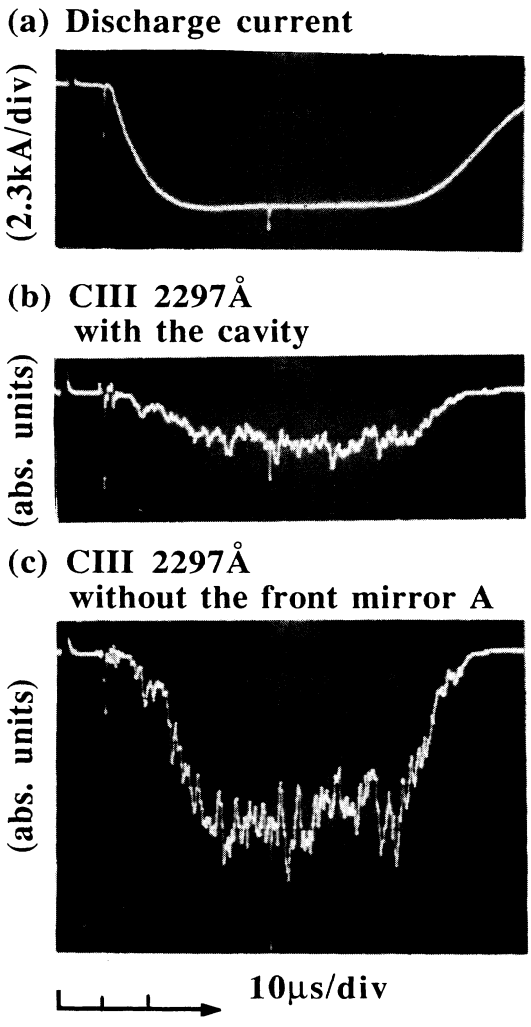

FIG. 27. Discharge current and spontaneous emission at 2297 Å in C III. (a) Discharge current. (b) C III–line emission at 2297 Å with the laser cavity. (c) C III–line emission at 2297 Å with the front mirror A removed.

To corroborate these measurements, similar measurements were made on the wing (optically thin) of the C III, $2p^2$-$2s2p$ line at 2297 Å. The upper level $2p^2$ of this line has no allowed transitions to either the upper or lower laser levels. No fluorescence, therefore, can occur on this line. For such a nonlasing line, the signal with the front mirror A removed should be *higher* than that with the tuned cavity. Figure 27(b) shows the measured cavity output of the spontaneous emission of this line, at a discharge current of 6.4 kA. The discharge current is shown in Fig. 27(a). The Mn pump plasma was produced 36 μs after carbon discharge initiation as indicated by the "noise" fiducial on all three traces in Fig. 27. No fluorescence was observed on this line as expected. Figure 27(c) shows the spontaneous emission, when the front cavity mirror A was removed. The measured signal was now *larger,* since the partially transmitting mirror A was removed from the line of sight. The measured signal at 2297 Å with the front mirror A removed was about five times *higher* than with the cavity, as expected. The dramatically *opposite* results obtained from a tuned cavity for the lasing lines at 2177 and 2163 Å as opposed to the nonlasing line at 2297 Å were encouraging. However it was still possible to hypothesize that the results of Fig. 26 might be due to radiation at 2177 and 2163 Å from the Mn pump plasma which "walks on" to the cavity, giving an apparent but spurious gain. To check this, the measurements were made with the Mn plasma alone (C discharge off). The measured signals with the front mirror A removed were about five times *higher* than with the cavity, i.e., the results were similar to those at the nonlasing wavelength of 2297 Å. Furthermore, the absolute levels of these signals were much smaller than those with the pumped carbon discharge, and thus did not influence the results of Fig. 26.

V. SUMMARY

In summary, the C III–Mn VI resonant photoexcited laser scheme has been analyzed and demonstrated. A model for the kinetics of the photoexcitation has been constructed. Spectroscopid diagnostics of the carbon plasma were presented. Enhanced fluorescence on the C III $4p$-$3d$, 2177-Å transition due to pumping by the Mn VI–line radiation has been observed. In addition, enhanced fluorescence has also been observed on other many $n=4$ to $n=3$ transitions in C III due to collisional coupling between the $n=4$ levels. Gain as high as 0.4 cm^{-1} has been measured at wavelengths of 2177 and 2163 Å in C III. Laser oscillation was demonstrated at these two wavelengths in a concentric Fabry-Perot resonator.

A rough estimate of the power and energy per pulse from those photoexcited lasers is obtained by assuming that the net gain coefficient is about 0.1 cm^{-1} (the measured single-pass gain was about 0.25 cm^{-1}). This gives an upper-level population ($4f$) of $\sim 10^{12}$ cm^{-3}. For a sa-

turated oscillator, the beam intensity in the active region is ~ 5 kW/cm^2. The output beam intensity is $\sim(1-r)\times 5$ kW/cm^2 $=400$ W/cm^2, where r $(=0.92)$ is the reflectivity of the cavity mirror. In the discharge, the active volume is about 1.0 cm in diameter by 2.0 cm long. The laser energy per pulse could be 0.1 mJ for a 300-ns duration. For a 6.4-kA discharge current, with a 0.05-Ω plasma impedance, the electrical energy input over 300 ns is 0.6 J. The CO_2 laser energy input to the Mn plasma is ~ 10 J. The CO_2 laser is not strictly necessary, because a fast capacitive discharge with ~ 10 J could also be used to produce the Mn VI–pump-line radiation,[52] with high efficiency. The overall efficiency of these photoexcited lasers is about (0.1 mJ)/(10 J) $\sim 10^{-5}$. It should be pointed out that the experimental configuration used is far from optimal. By making the pump plasma coaxial with the laser medium, a greater solid angle can be utilized for photoexcitation, increasing the gain, and hence the efficiency. It is possible that soft-x-ray analogs of the C III–Mn VI laser described here could be produced, with similar overall efficiencies.

Laser action at wavelengths of 2177 and 2163 Å in C III has been demonstrated. It is of interest and importance to translate these results to shorter wavelengths, in isoelectronic analogs of C III. A computer simulation of the N VI–P IX scheme[37] was carried out. The method which was described in Sec. II was used for the modeling. In the CR model, which calculates populations of the excited states in N IV, the transition probabilities were scaled by assuming that oscillator strengths are the same for C III and N IV ions; Collisional excitation and deexcitation rates were derived from oscillator strengths; ionization and recombination rates are from the same sources as that for C III ions. The maximum fractions for N IV and P IX ions occur at $T_e=9$ and 90 eV, respectively. Assuming a 45-eV brightness temperature for the P IX–pump-line intensity, the calculated gain for the $4p$-$3d$ transition in N IV is about 0.7 cm^{-1} at pumped nitrogen plasma conditions of $N_e=5\times 10^{16}$ cm^{-3} and $T_e=8$ eV. Again, such plasma conditions could be prepared in a gas discharge for the pumped nitrogen plasma and in a laser-produced plasma for the pumped phosphorus plasma. Lasing is possible on several $n=4$ to $n=3$ transitions in N IV, from 1284- to 948-Å wavelengths. A detailed experimental study of the N IV–P IX scheme would shed light on possible soft-x-ray lasers at 230 Å in Mg IX.

ACKNOWLEDGMENTS

The research support of U.S. Air Force Office of Scientific Research (Grant No. 81-0077) is gratefully acknowledged. The interest of Dr. Michael A. Stroscio and later of Dr. Robert Barker was important and encouraged us throughout this research. The generosity of Dr. W. L. Morgan made it possible for us to make use of atomic physics data from Livermore Laboratories. Dr. S. Suckewer and his group at Princeton Plasma Physics Laboratory helped us to calibrate the 0.2-m spectrometer. The work evolved from ideas of pioneering studies by Dr. James E. Trebes. We also acknowledge many helpful discussions with Dr. R. R. Prasad and his assistance in constructing the coronal ionization balance. Dr. H. Kilic participated in some aspects of this research, especially in the establishment of the scale length for opacity estimates and emission-line-profile measurements.

*Present address: Laboratory of Plasma Studies, 369 Upson Hall, Cornell University, Ithaca, NY 14853-7501.

†Present address: Physics International Co., San Leandro, CA 94577.

[1]G. Chapline and L. Wood, Phys. Today **6**, 41 (1975).

[2]R. W. Waynant and R. C. Elton, Proc. IEEE **64**, 1059 (1976).

[3]P. L. Hagelstein, in *Atomic Physics 9*, Proceedings of the Ninth International Conference on Atomic Physics, Seattle, 1984, edited by R. S. Van Dyck and E.N. Fortson (World Scientific, Singapore, 1984), p. 382.

[4]J. Apruzese, Eur. Sci. Notes **40**, 283 (1986).

[5]D. Nagel, Naval Research Laboratory Report No. 4465, 1981 (unpublished).

[6]*Short Wavelength Coherent Radiation: Generation and Applications*, edited by D. Attwood and J. Bokor (AIP, New York, 1986).

[7]J. Trebes, J. Phys. (Paris) Colloq. Suppl. 10 **47**, C6-309 (1986).

[8]R. C. Elton, Appl. Opt. **14**, 97 (1975).

[9]A. N. Zherikhin *et al.*, Kvant. Elektron. (Moscow) **3**, 152 (1976) [Sov. J. Quantum Electron. **6**, 82 (1976)].

[10]P. Hagelstein, Ph.D. thesis, Massachusetts Institute of Technology Report No. UCRL-53100, 1981 (unpublished).

[11]S. Maxon, P. Hagelstein, K. Reed, and J. Scofield, J. Appl. Phys. **57**, 971 (1985); P. L. Hagelstein, Phys. Rev. A **34**, 874 (1986).

[12]L. I. Gudzenko and L. A. Shelepin, Zh. Eksp. Teor. Fiz. **45**, 1445 (1963) [Sov. Phys.—JETP **18**, 998 (1964)]; Dokl. Akad. Nauk SSSR **160**, 1296 (1965) [Sov. Phys.—Dokl. **10**, 147 (1965)].

[13]G. J. Pert, J. Phys. B **37**, 3301 (1976); **12**, 2067 (1979).

[14]S. Suckewer and H. Fishman, J. Appl. Phys. **54**, 1922 (1980).

[15]G. Jamelot, A. Klisnick, A. Carillon, H. Guennou, A. Sureau, and P. Jaegle, J. Phys. B **18**, 4647 (1985).

[16]J. P. Apruzese, J. Davis, P. C. Kepple, and M. Blaha, J. Phys. (Paris) Colloq. Suppl. **10**, 47 C6-15 (1986).

[17]M. A. Duguay and P. M. Rentzepis, Appl. Phys. Lett. **10**, 350 (1967).

[18]P. L. Hagelstein, Lawrence Livermore National Laboratory Report No. UCID-17629, 1977 (unpublished).

[19]W. T. Silfvast, in *Laser Techniques in the Extreme Ultraviolet, OSA, Boulder, Colorado, 1984*, edited by S. E. Harris and T. B. Lucatorto (AIP, New York, 1984), p. 427.

[20]A. V. Vinogradov, I. I. Sobelman, and E. A. Yukov, Kvant. Elektron. (Moscow) **2**, 105 (1975) [Sov. J. Quantum Electron. **5**, 59 (1975)].

[21]B. A. Norton and N. J. Peacock, J. Phys. B **8**, 989 (1973).

[22]J. P. Apruzese, J. Davis, and K. G. Whitney, J. Phys. B **11**, L643 (1978); J. Appl. Phys. **53**, 4020 (1982).

[23]D. L. Matthews *et al.*, Phys. Rev. Lett. **54**, 110 (1985).

[24]T. N. Lee, E. A. McLean, and R. C. Elton, Phys. Rev. Lett. **59**, 1185 (1987).

[25]B. J. MacGowan *et al.*, Phys. Rev. Lett. **59**, 2157 (1987).

[26]S. Suckewer *et al.*, Phys. Rev. Lett. **55**, 1753 (1985).

[27]J. F. Seely, C. M. Brown, U. Feldman, M. Richardson, B.

Yaakobi, and W. E. Behring, Opt. Commun. **54**, 289 (1985).
[28]P. Jaegle, G. Jamelot, and A. Klisnick, J. Phys. (Paris) Colloq. Suppl. 10 **47**, C6-31 (1986).
[29]C. Chenais-Popovics, R. Corbett, C. J. Hooker, M. H. Key, G. P. Kiehn, C. L. S. Lewis, G. J. Pert, C. Regan, S. J. Rose, S. Sadaat, R. Smith, T. Tomie, and O. Willi, Phys. Rev. Lett. **59**, 2161 (1987).
[30]C. Boeckner, J. Res. Nat. Bur. Stand. **5**, 13 (1930).
[31]S. Jacobs, G. Gould, and P. Rabinowitz, Phys. Rev. Lett. **7**, 415 (1961).
[32]V. N. Lisitsyn, A. I. Fedchenko, and V. P. Chebotayev, Opt. Spectrosc. (USSR) **27**, 157 (1969).
[33]N. Djeu and R. Burnham, Appl. Phys. Lett. **25**, 350 (1974).
[34]V. Bhagavatula, J. Appl. Phys. B **11**, 1643 (1978).
[35]D. L. Matthews *et al.*, IEEE J. Quantum Electron. **QE-19**, 1786 (1983).
[36]J. P. Apruzese, G. Mehlman, J. Davis, J. E. Rogerson, V. E. Scherrer, S. J. Stephanakis, P. F. Ottinger, and F. C. Young, Phys. Rev. A **35**, 4896 (1987).
[37]M. Krishnan and J. Trebes, Appl. Phys. Lett. **45**, 189 (1984).
[38]K. L. Bell, H. B. Gilbody, J. G. Hughes, A. E. Kinkston, and F. J. Smith, J. Phys. Chem. Ref. Data **12**, 891 (1983).
[39]Y. Zel'dovich and Y. Raizer, *Physics of Shock Waves and High Temperature Hydrodynamic Phenomena* (Academic, New York, 1967), Vol. 1.
[40]S. M. V. Aldrovandi and D. Pequinot, Astron. Astrophys. **25**, 137 (1973).
[41]A. Burgess, Astrophys. J. **141**, 1588 (1965).
[42]D. L. Moores, L. B. Golden, and D. H. Sampson, J. Phys. B **13**, 385 (1980).
[43]L. B. Golden and D. H. Sampson, J. Phys. B **13**, 2645 (1980).
[44]R. E. H. Clark and D. H. Sampson, J. Phys. B **17**, 3311 (1984).
[45]D. R. Bates, A. E. Kingston, and R. W. P. McWhirter, Proc. R. Soc. London, Ser. A **267**, 297 (1962); **270**, 155 (1962).
[46]T. Holstein, Phys. Rev. **72**, 1212 (1947).
[47]T. Holstein, Phys. Rev. **83**, 1159 (1951).
[48]H. R. Griem, *Plasma Spectroscopy* (McGraw-Hill, New York, 1964).
[49]W. L. Morgan (private communication).
[50]L. Vriens and A. H. M. Smeets, Phys. Rev. A **22**, 940 (1980).
[51]M. J. Seaton, in *Atomic and Molecular Processes,* edited by D. R. Bates (Academic, New York, 1962), Chap. 11.
[52]N. Qi, Ph.D. thesis, Yale University, New Haven, Connecticut 1987 (unpublished).
[53]R. D. Cowan, *The Theory of Atomic Structure and Spectra* (University of California Press, Berkeley, 1981), p. 406.
[54]N. Konjevic and R. J. Roberts, J. Phys. Chem. Ref. Data **5**, 209 (1976).
[55]B. H. Armstrong, J. Quant. Spectrosc. Radiat. Transfer **7**, 61 (1967).
[56]H. R. Griem, *Spectral Line Broadening by Plasma* (Academic, New York, 1974).
[57]H. J. Kusch, Z. Astrophys. **67**, 64 (1976).
[58]P. Bogen, Z. Naturforsch. Teil A **27**, 210 (1972).
[59]R. M. Nasser and Y. P. Varshni, Astron. Astrophys., Suppl. Ser. **60**, 325 (1985).
[60]N. Qi and M. Krishnan, Phys. Rev. Lett. **59**, 2051 (1987).

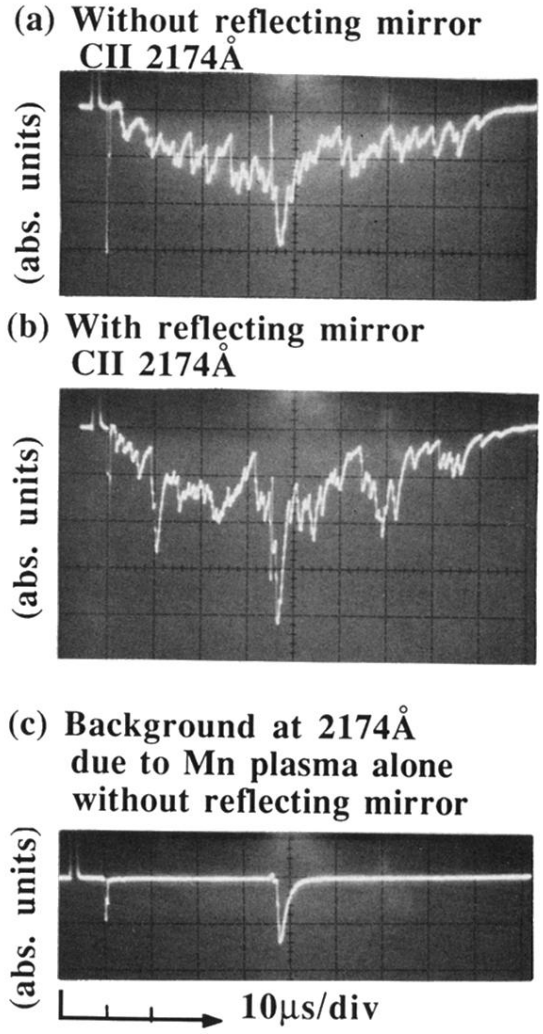

FIG. 23. Calibration experiment for single-pass gain measurement. (a) and (b) are spontaneous emission at 2174 Å in C II detected without and with the reflecting mirror, respectively. (c) Spurious background at 2177 Å due to the laser-produced Mn plasma alone.

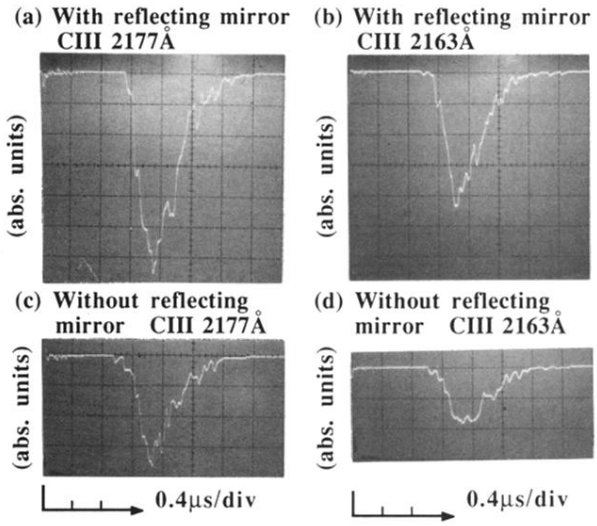

FIG. 24. Single-pass gain at 2177 and 2163 Å in C III. (a) and (c) are enhanced fluorescence, with the reflecting mirror, at 2177 and 2163 Å, respectively. (b) and (d) are enhanced fluorescence, without the reflecting mirror, at 2177 and 2163 Å, respectively.

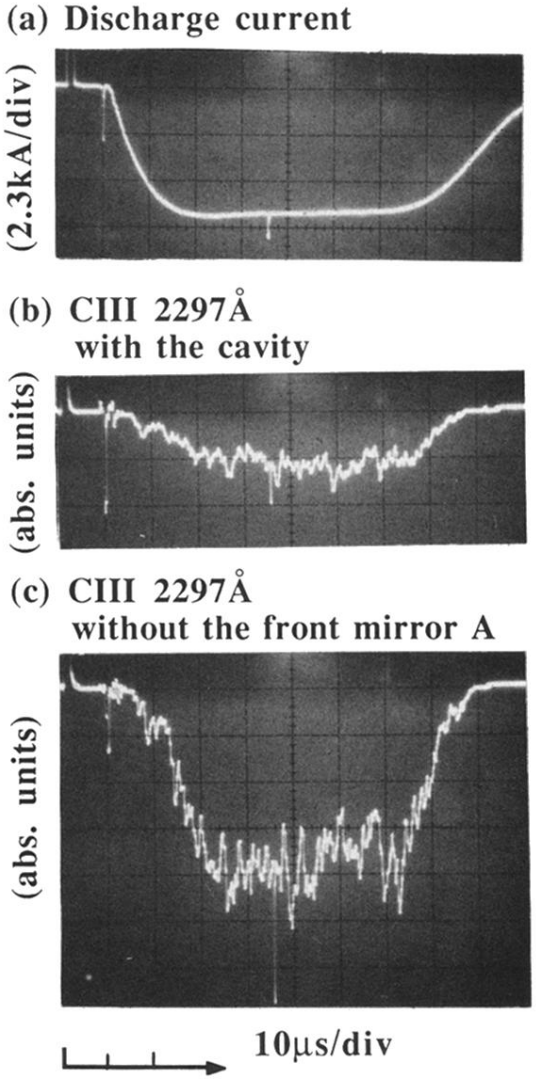

FIG. 27. Discharge current and spontaneous emission at 2297 Å in C III. (a) Discharge current. (b) C III–line emission at 2297 Å with the laser cavity. (c) C III–line emission at 2297 Å with the front mirror *A* removed.

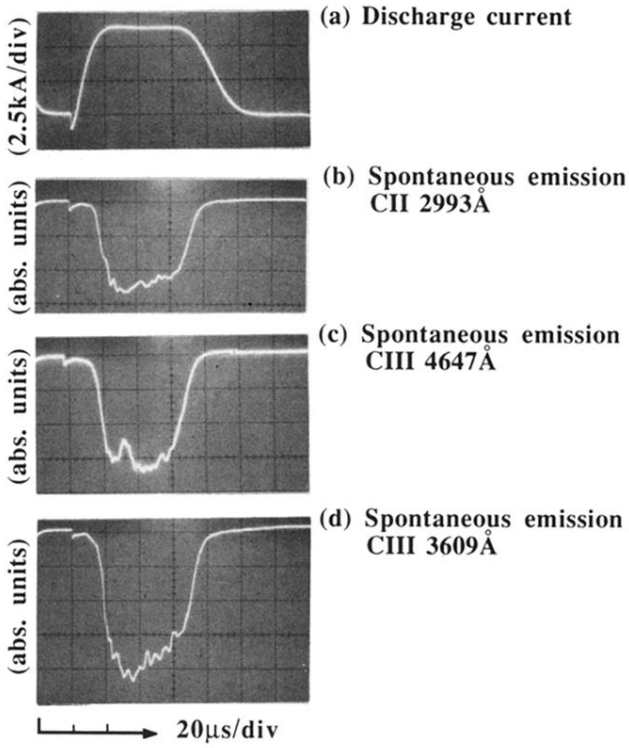

FIG. 9. Line intensities of carbon ions vs time.